Zero-Speed Operation of High-Power PWM Current-Source-Inverter-Fed Induction Motor Drive

Fangrui Liu, *Member, IEEE*, Bin Wu, *Fellow, IEEE*, Manish Pande, *Member, IEEE*, and Navid Reza Zargari, *Senior Member, IEEE*

***Abstract*—Most research work in current-source inverter (CSI) fed motor drives has focused on general control strategies, pulsewidth modulation schemes, topologies, and efficiency evaluation. This paper, however, is dedicated to investigating zero-speed operation characteristics of CSI-fed induction motor drives (IMDs). Zero-speed operation can greatly increase the competitive value of the drive and expand its range of applications to include cranes, hoists, and draglines. The motor drive is controlled with rotor flux orientation, where stator currents and motor speed are employed for the rotor flux estimation. Unlike voltage-source-inverter-based drives, filter capacitors are required at the output of the CSI for current commutation and harmonics filtering. The influence of these capacitors on the system dynamic performance is comprehensively evaluated. Moreover, a classic load torque observer with feedforward control is employed to improve the speed dynamic response. Simulated and experimental results show that the CSI-fed IMD works well at zero speed with promising speed dynamic performance.**

***Index Terms*—Current-source inverter (CSI), induction motor drive (IMD), zero speed.**

NOMENCLATURE

C_f	Motor-side filter capacitance.
e_d, e_q	Motor back electromotive force (*EMF*) in the *dq* reference frame.
i_{cd}, i_{cq}	Motor-side capacitor current in the *dq* reference frame.
$i_{\rm dc}$, $i^*_{\rm dc}$	DC-link current and its reference.
$i_s = (i_{\alpha s}\ i_{\beta s})^T$	Stator current in the $\alpha\beta$ reference frame.
i^*_{ds}, i^*_{qs}	Stator reference current in the *dq* reference frame.
i^*_{dw}, i^*_{qw}	Inverter reference current in the *dq* reference frame.
J	Inertia of motor and its load.
K_t	Equivalent torque constant.
$L_{\rm dc}$	DC-link inductance.
L_m	Magnetizing inductance.
L_s, L_r	Self-inductance of stator and rotor.
T_{di}	Inverter processing delay.
T_e, T^*_e	Electromagnetic torque and its reference.
$\hat{T}_L$	Estimated load torque.
v_{ds}, v_{qs}	Stator voltage in the *dq* reference frame.
$\lambda_{\alpha r}$, $\lambda_{\beta r}$	Rotor flux linkage in the $\alpha\beta$ reference frame.
λ_{dr}, λ_{qr}	Rotor flux linkage in the *dq* reference frame.
λ_r, λ^*_r	Magnitude of rotor flux linkage and its reference.
ω_e	Motor electrical frequency.
ω_r, ω^*_r	Motor speed and its reference.
σ	Motor total leakage factor.
τ	Time constant of a low-pass filter.
τ_r	Rotor time constant.
θ_f	Angle of rotor flux linkage.
θ_{inv}	Inverter firing angle.
θ_w	Angle of inverter reference current.

I. INTRODUCTION

SIMPLE converter structure, motor-friendly waveforms, inherent four-quadrant operation capability, and reliable short-circuit protection are features that make current-source inverter (CSI) well suited for medium-voltage drives applications [1]. By adopting gate-turn-OFF thyristers or gate-commutated thyristers (GCTs, for example, integrated GCT [2], symmetrical GCT [3]) as switching devices, pulsewidth-modulated (PWM) current-source converters can achieve improved line/load current harmonics, superior power factor, and reduced costs with the possibility of eliminating the input transformer [1]–[4]. Field-oriented control strategies are widely employed in the high-power current-source drives to improve system dynamics and reliability.

Recent work has focused on control strategies [5]–[9], PWM schemes [10]–[13], topologies [14]–[17], and efficiency [18], [19] for high-power current-source converters and drives, where significant improvements have been achieved, such as harmonic distortion minimization, high input power factor, minimized dc-link current, and reduced switching frequencies. However, it seems that zero-speed operation of the high-power PWM CSI-fed induction motor drive (IMD) has seldom been reported. Zero-speed operation plays an important role in applications such as cranes, hoists, and traction drives, where maintaining the desired torque down to zero speed or starting the load with a high torque from zero speed is highly desirable. This paper is

Manuscript received March 24, 2011; revised August 14, 2011; accepted October 30, 2011. Date of current version March 16, 2012. Recommended for publication by Associate Editor J. R. Rodriguez.

F. Liu is with the Department of Electrical and Computer Engineering, Ryerson University, Toronto, ON M5B 2K3, Canada (e-mail: fangruiwh@gmail.com)

B. Wu is with Ryerson University, Toronto, ON M5B 2K3, Canada (e-mail: bwu@ee.ryerson.ca).

M. Pande and N. R. Zargari are with the Medium Voltage R&D Department, Rockwell Automation, Cambridge, ON N1R 5X1, Canada (e-mail: mpande@ra.rockwell.com; nrzargari@ra.rockwell.com).

Color versions of one or more of the figures in this paper are available online at http://ieeexplore.ieee.org.

Digital Object Identifier 10.1109/TPEL.2011.2176542

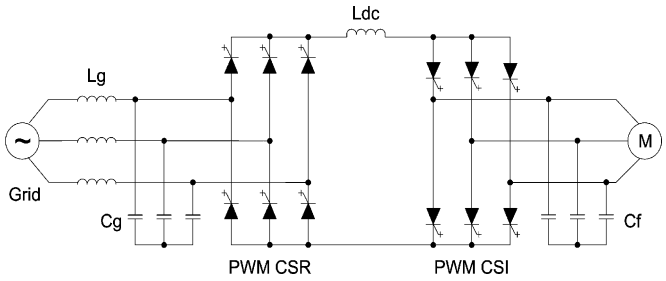

Fig. 1. PWM current-source converter-based motor drive.

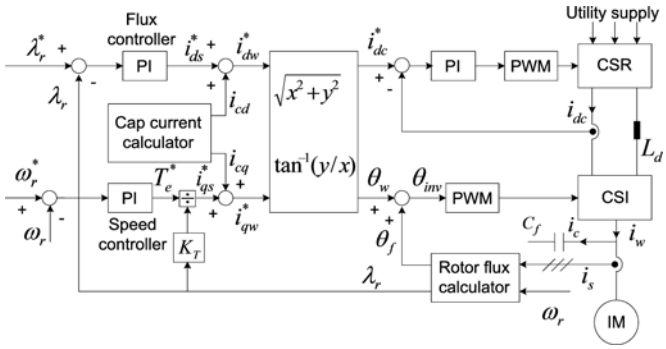

Fig. 2. Motor control scheme.

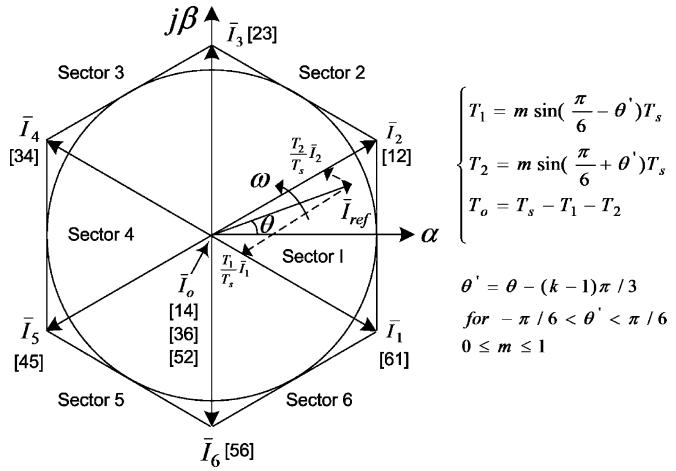

Fig. 3. Space vector and synthesis for CSI [20].

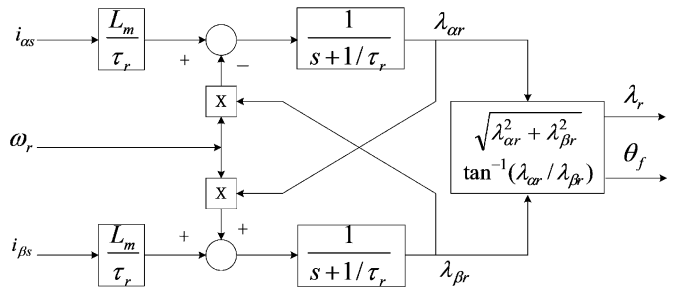

Fig. 4. Current flux model.

therefore dedicated to exploring the zero-speed operation characteristics of the PWM CSI-fed IMDs.

In this paper, the drive is controlled with rotor flux field orientation, where the flux is identified by current model. In the system structure shown in Fig. 1, filter capacitors are connected at the output of the CSI to assist with current commutation and harmonics filtering. Thus, the inverter d, q-axis currents are different from the stator d, q-axis currents. The impact of the capacitors on the drive dynamic performance is systematically analyzed. Moreover, a classic load torque observer with feedforward control is adopted to improve the speed dynamic response. Simulation and experimental results show that the CSI-fed IMD works well at zero speed with promising speed dynamic performance.

II. System Control Scheme

A. Motor Control Scheme

The induction motor control scheme is shown in Fig. 2, where rotor flux orientation is employed [20]. The flux and speed controllers are utilized to generate the motor d-axis current (i_{ds}^*) and q-axis current (i_{qs}^*), respectively. The sum of stator d, q-axis currents and the compensated capacitor currents is used to produce the inverter reference d, q-axis currents (i_{dw}^* and i_{qw}^*). In order to minimize the dc-link current, the amplitude ($i_{\rm dc}^*$) of the synthesized inverter reference current is served as the reference for dc-link current control of the current source rectifier, while the corresponding phase θ_w is added to the rotor flux angle θ_f for the modulation of the CSI.

There are several ways to implement the modulation for the CSI, including mapping method from voltage-source inverter modulation [21], space vector modulation, and so on. The space vector modulation shown in Fig. 3 is employed where active and zero vectors are calculated. The typical three-segment sequence is then used to obtain the gating signals for each switching devices [20]. The corresponding advantages include a reduction in switching frequency, which leads to a reduction in switching losses, and reduced complexity for switching scheme implementation. A fixed modulation index of 1 is adopted for the CSI to reduce the dc-link current and operating losses.

B. Current Flux Model

The current model is utilized for the flux estimation, where the rotor flux components can be synthesized easily with the help of speed and current signals. The relationship among the rotor flux ($\lambda_{\alpha r}, \lambda_{\beta r}$), stator current ($i_{\alpha s}, i_{\beta s}$), and motor speed ($\omega_r$) in two-phase stationary reference frame is shown as follows [22]:

$$\begin{cases} \left(p + \dfrac{1}{\tau_r}\right)\lambda_{\alpha r} = \dfrac{L_m}{\tau_r} i_{\alpha s} - \omega_r \lambda_{\beta r} \\ \left(p + \dfrac{1}{\tau_r}\right)\lambda_{\beta r} = \dfrac{L_m}{\tau_r} i_{\beta s} + \omega_r \lambda_{\alpha r} \end{cases} \tag{1}$$

where $\tau_r = L_r/R_r$ is the rotor circuit time constant, and p is the derivative operator. The corresponding flux estimation diagram is shown in Fig. 4.

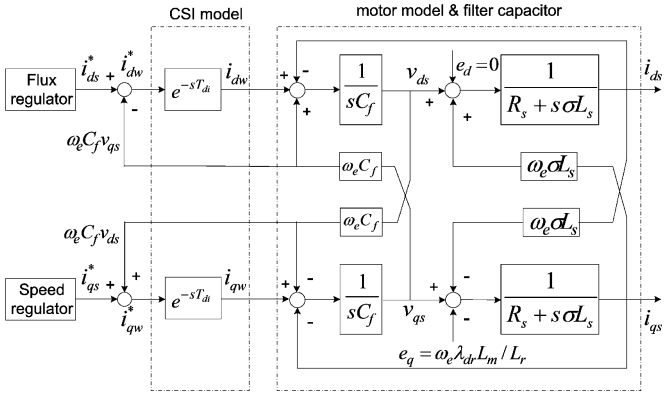

Fig. 5. Control block of the CSI and the induction motor.

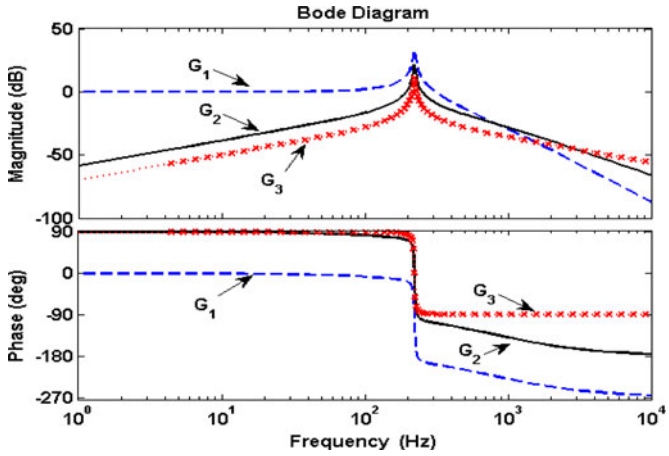

Fig. 6. Bode diagrams of G_1, G_2, and G_3.

III. Impact of Filter Capacitor on System Control

CSI-fed motor drives have filter capacitors connected at the output of the inverter. This means that a portion of the inverter currents go through the capacitors. The influence of the filter capacitors on the system control is investigated in this section.

A. Coupling Analysis of Stator d, q-Axis Currents

As mentioned previously, the inverter reference currents can be expressed as follows [20]:

$$\begin{cases} i_{dw}^* = i_{cd} + i_{ds}^* \\ i_{qw}^* = i_{cq} + i_{qs}^* \end{cases} \tag{2}$$

where i_{cd} and i_{cq} are the estimated capacitor d, q-axis currents. To reduce the sensitivity and noise caused by the derivative terms, the estimated capacitor currents are usually simplified as follows:

$$\begin{cases} i_{cd} = -\omega_e v_{qs} C_f \\ i_{cq} = \omega_e v_{ds} C_f \end{cases} \tag{3}$$

where C_f, ω_e, v_{ds}, and v_{qs} are the inverter-side filter capacitance, motor electrical angular frequency, and stator d-axis and q-axis voltages, respectively.

The stator voltage equations of induction machine in synchronous reference frame can be expressed as follows [23]:

$$\begin{bmatrix} v_{ds} \\ v_{qs} \end{bmatrix} = \begin{bmatrix} s\sigma L_s + R_s & -\omega_e \sigma L_s \\ \omega_e \sigma L_s & s\sigma L_s + R_s \end{bmatrix} \begin{bmatrix} i_{ds} \\ i_{qs} \end{bmatrix} + \begin{bmatrix} e_d \\ e_q \end{bmatrix} \tag{4}$$

where σ, e_d, and e_q are the induction motor total leakage factor $(1 - L_m^2/(L_s L_r))$, and d- and q-axis back electromotive force (*EMF*), respectively. Under rotor flux orientation, the rotor flux vector is aligned with the d-axis and its amplitude is kept constant. Thus, the induction motor back *EMF* can be obtained as follows:

$$\begin{cases} e_d = 0 \\ e_q = \dfrac{\omega_e \lambda_{dr} L_m}{L_r}. \end{cases} \tag{5}$$

With the rotor flux orientation control, the detailed current controlled diagram of induction motor and the inverter is shown in Fig. 5, where T_{di} is the inverter processing delay. The rotor flux controller and speed controller provide the motor d, q-axis reference currents i_{ds}^* and i_{qs}^*, respectively. After the capacitor current compensation, the inverter reference currents i_{dw}^* and i_{qw}^* are generated. Subsequently, the inverter real currents i_{dw} and i_{qw} can be obtained with an inverter processing delay of T_{di} and then supply the filter capacitor and motor. For the system shown in Fig. 5, the motor d, q-axis reference currents and real currents can be considered as input and output, respectively, and the following equation can be obtained:

$$\begin{cases} i_{ds} = G_1 i_{ds}^* + G_2 \omega_e C_f v_{qs} + G_3 \omega_e \sigma L_s i_{qs} \\ i_{qs} = G_1 i_{qs}^* - G_2 \omega_e C_f v_{ds} - G_3 \omega_e \sigma L_s i_{ds} - G_3 e_q \end{cases} \tag{6}$$

where $G_1 = (1/1 + sT_{di})G_0, G_2 = (sT_{di}/1 + sT_{di})G_0, G_3 = sC_f G_0$, and $G_0 = (1/1 + R_s C_f s + \sigma L_s C_f s^2)$.

As can be seen from (6), the gains of coupling terms between stator d, q-axis currents are proportional to the motor electrical frequency ω_e. When operating at low and zero speed, the electrical frequency of high-power induction motor is considerably small. Bode diagrams of transfer functions for these coupling terms are shown in Fig. 6.The gains of G_2 and G_3 in (6) can be seen less than -40 db for frequencies below 6 Hz. Due to the high attenuation capability, the coupling terms of the capacitor voltages, motor currents, and back *EMF* can be eliminated quickly under zero and low-speed operation (e.g., less than 0.1 p.u.).

B. CSI Reference Current Adaptability to the Variation of Electrical Frequency

Since the motor speed is measured by the speed encoder, the motor electrical frequency can be estimated by the following equation [20]:

$$\omega_e = \omega_r + \frac{L_m}{\tau_r \lambda_r} i_{qs}. \tag{7}$$

The motor parameters employed in the control system may deviate from the real ones. Thus, ω_e may not be accurately obtained. In the following, the impact of ω_e on the inverter reference current will be evaluated.

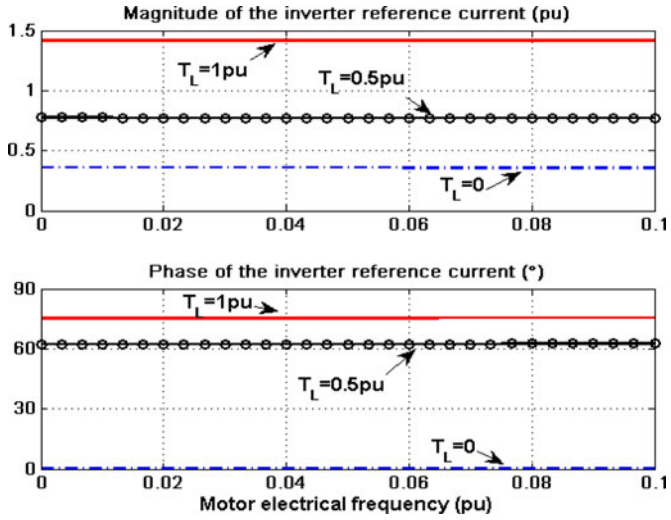

Fig. 7. Inverter reference current magnitude and phase under different ω_e.

By substituting the motor reference voltage into (2), the inverter reference current can be expressed as follows:

$$\begin{cases} i_{dw}^* = i_{cd} + i_{ds}^* = i_{ds}^* - \omega_e C_f R_s i_{qs}^* - \omega_e^2 C_f \dfrac{L_m}{L_r}\lambda_{dr} \\ \qquad - \omega_e^2 C_f \sigma L_s i_{ds}^* \\ i_{qw}^* = i_{cq} + i_{qs}^* = i_{qs}^* + \omega_e C_f R_s i_{ds}^* - \omega_e^2 C_f \dfrac{L_m}{L_r}\lambda_{qr} \\ \qquad - \omega_e^2 C_f \sigma L_s i_{qs}^*. \end{cases} \tag{8}$$

Considering the rotor flux orientation, the above equation can be simplified as follows:

$$\begin{cases} i_{dw}^* = i_{ds}^* - \omega_e C_f R_s i_{qs}^* - \omega_e^2 C_f \dfrac{L_m}{L_r}\lambda_r - \omega_e^2 C_f \sigma L_s i_{ds}^* \\ i_{qw}^* = i_{qs}^* + \omega_e C_f R_s i_{ds}^* - \omega_e^2 C_f \sigma L_s i_{qs}^*. \end{cases} \tag{9}$$

Using (9), the inverter reference current vector as a function of motor electrical frequency ω_e can be shown in Fig. 7. For the same load torque, the inverter reference current magnitude and phase can be seen varying little as the frequency increases. This means that the estimation error of electrical frequency does not significantly affect the inverter reference current. Therefore, the system control has a good adaptability to the estimation error of the electrical frequency. Moreover, almost same magnitude and phase of the reference current at 0 and 0.1 p.u. motor electrical frequency further illustrates that neglecting the influence of the capacitor for the stator current control causes little errors for zero- and low-speed operation.

IV. Improvement of Speed Dynamic Performance

Referring to Fig. 2, the CSI modulation index is fixed at 1 and the stator current amplitude is regulated by varying the dc-link current. With a considerably large dc-link current, the CSI modulation index control may improve the speed dynamic performance; however, the losses will increase. Therefore, the load torque feedforward control is employed as a compromise.

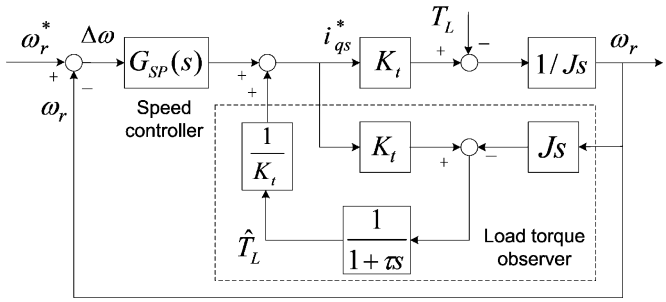

Fig. 8. Speed control block diagram with classic load torque feedforward control [24].

The classic load torque disturbance feedforward compensation scheme [24] is shown in Fig. 8. The estimated load torque $\hat{T}_L$ is calculated according to the motor's mechanical equation as follows:

$$\hat{T}_L \approx K_t i_{qs}^* - Js\omega_r \tag{10}$$

where J is the inertia of the motor and load, and K_t is the equivalent torque constant with definition as follows:

$$K_t = \frac{3P}{2}\lambda_r \tag{11}$$

where P the number of pole pairs. Considering the HF harmonics and noises presented in the measured speed signal, a low-pass filter with time constant of τ is employed to filter the estimated load torque $\hat{T}_L$. After dividing by the equivalent torque constantK_t, the estimated load torque $\hat{T}_L$ is fed forward in the controller.

When the parameters K_t and J used in the load torque observer are the same as the actual ones, the input to output transfer functions can be expressed as follows:

$$\frac{\omega_r}{\omega_r^*} = \frac{K_t G_{sp}(s)}{sJ + K_t G_{sp}(s)} \tag{12}$$

$$\frac{\omega_r}{T_L} = -\frac{\tau s}{1+\tau s}\frac{1}{sJ + K_t G_{sp}(s)}. \tag{13}$$

The prominent characteristic of the control scheme in Fig. 8 is the good adaptability to parameter variation [24].

V. Simulation and Experimental Results

In order to illustrate the feasibility of the zero-speed operation control scheme, a CSI-based ac drive model is developed with MATLAB/Simulink to feed a 1250-hp 4160-V six-pole induction motor. System parameters are shown in Table I. The control scheme presented in Fig. 2 is employed for the drive system.

The drive performance under step torque variation is shown in Fig. 9. The stator flux is initially established through dc current, while the stator q-axis current is zero. At 0.6 s, a rated load torque is suddenly addressed and the stator q-axis current is increased to handle it. The stator d-axis current varies a little and recovers quickly. This verifies that the coupling between stator d, q-axis currents has negligible impact on the system control. The motor

TABLE I
SYSTEM PARAMETERS

Converters	
Grid voltage: 4160 V (line to line), 60 Hz	Grid-side capacitor: 66.2 uF (0.4 pu)
Dc inductance: 42.5 mH (1 pu)	Motor-side capacitor: 63 uF (0.38 pu)
Switching frequency: 540 Hz (CSR and CSI)	
Induction motor	
Rated voltage: 4160 V (line to line)	Stator self inductance: 160.2 mH (3.77 pu)
Rated current: 150 A	Rotor resistance: 0.146 Ω (0.00912 pu)
Pole pairs: 3	Rotor self inductance: 160.2 mH (3.77 pu)
Moment of inertia: 440 kg.m^2	Magnetizing inductance: 155 mH (3.65 pu)
Rated torque: 7490 N.m	Rated speed: 1189 rpm

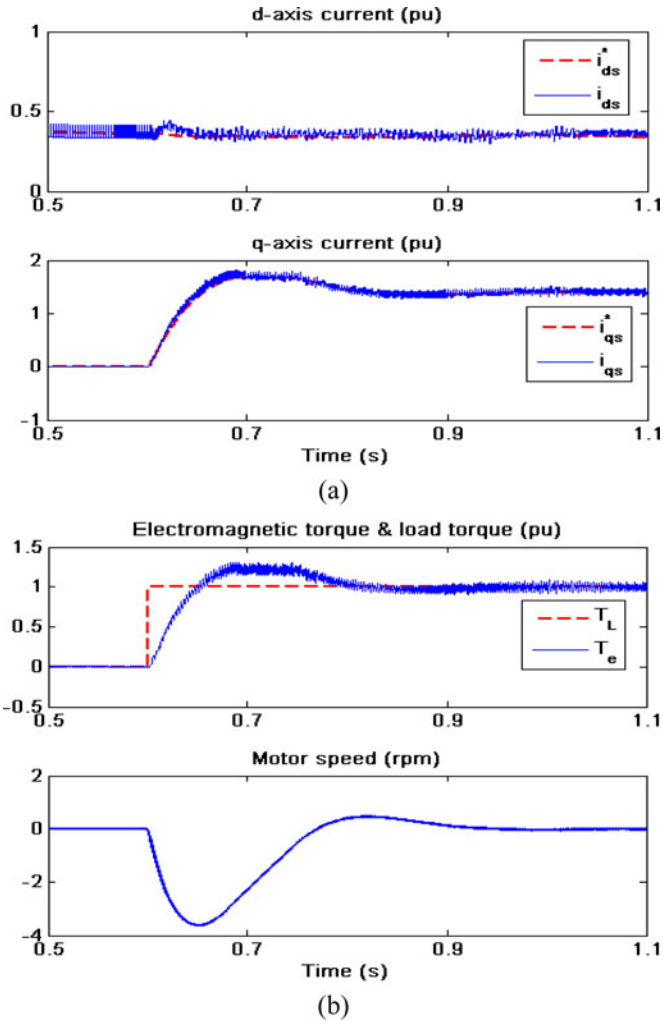

Fig. 9. Motor performance under step load torque variation. (a) Stator d, q-axis currents. (b) Torque and speed.

speed drops 3.6 r/min and goes back to steady state within 0.3 s. It is worth mentioning that the time constant of the motor is around 3.5 s. Thus, the speed drop here is not obvious.

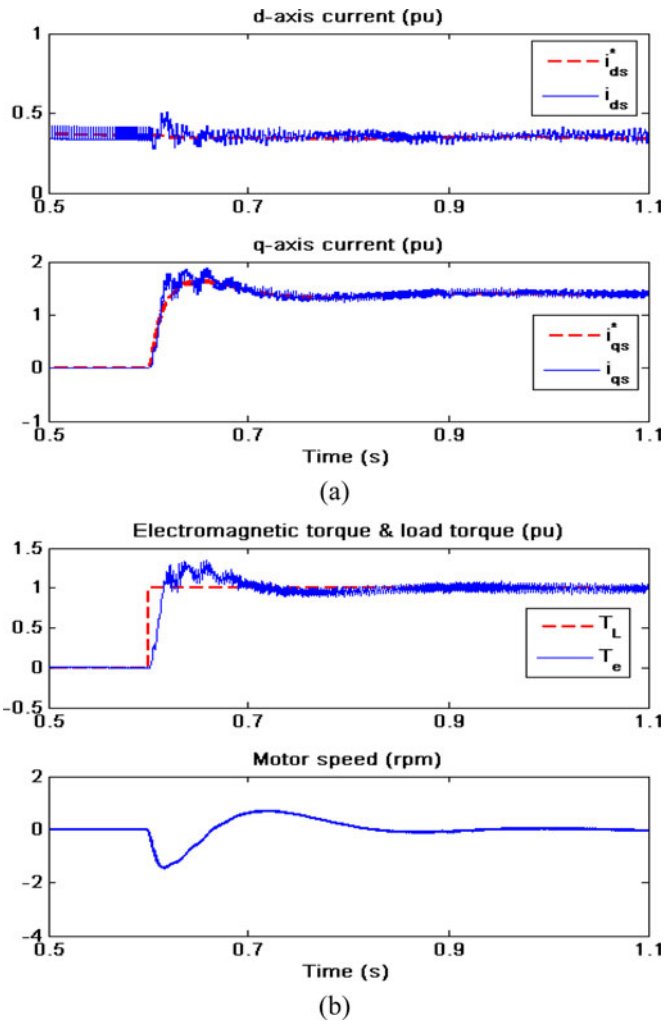

Fig. 10. Motor performance under step load torque variation (with load torque feedforward control). (a) Stator d, q-axis currents. (b) Torque and speed.

In order to improve the system dynamic performance, the load torque feedforward control is employed. The corresponding system waveforms are shown in Fig. 10. With the load torque feedforward control, the stator q-axis reference current [see Fig. 10(a)] responds faster to the load torque variation and the real q-axis current exhibits a little transient oscillation. Referring to (6), the faster variation of the q-axis current will increase the coupling effect on the d-axis current. This is the reason that the stator d-axis current in Fig. 10(a) exhibits more transient resonance than its counterpart in Fig. 9(a). Nevertheless, the resonance is small and diminishes quickly. In Figs. 9 and 10, the speed controller parameters are the same. With the load torque feedforward control, the motor speed drop is reduced from 3.6 to 1.5 r/min with slight increase of the speed recovery overshoot.

Digital simulation is also carried out for different moment of inertia used in the load torque observer to investigate the controller adaptability, and the corresponding torque and speed response is shown in Fig. 11. Compared with Fig. 10(b), the torque and speed performance with 50% deviation of the moment of inertia in the algorithm is still acceptable.

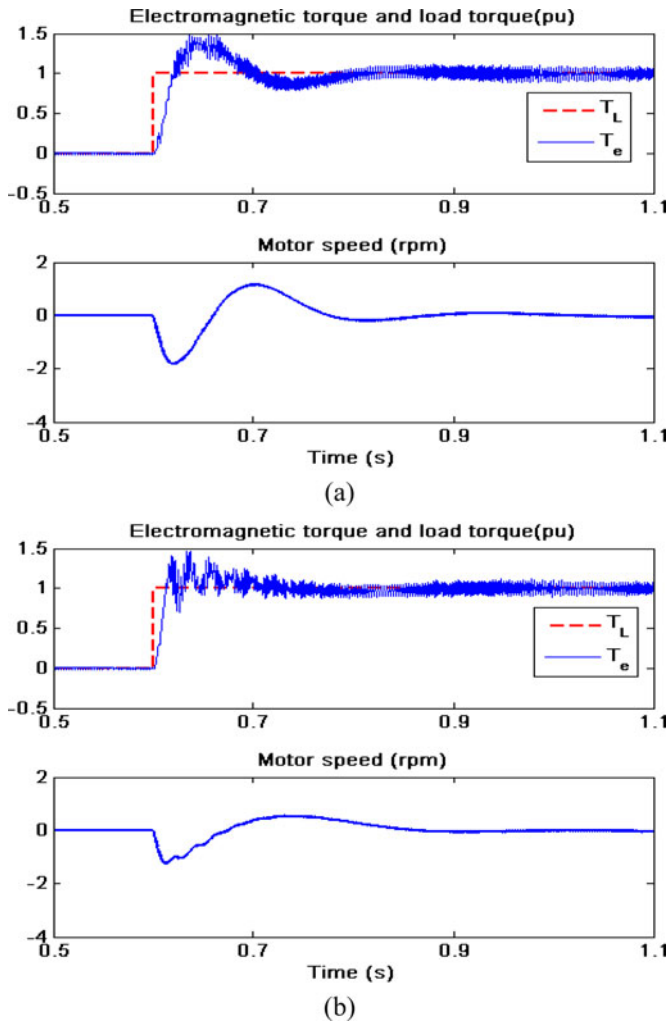

Fig. 11. Torque and speed response with different moment of inertia set in the load torque observer. (a) 50% of J. (b) 150% of J.

TABLE II
KEY PARAMETERS OF THE EXPERIMENT SETUP

Dc inductance: 30 mH (1 pu)	Grid-side capacitor: 90 uF (0.4 pu)
Switching frequency: 540 Hz	Motor-side capacitor: 100 uF (0.45 pu)
Motor power: 3 kW	Rated speed: 1700 rpm
Moment of inertia: 0.15 kg.m^2	Rated torque: 16.9 N.m

A low-power prototype system is constructed for experimental verification with key parameters listed in Table II. Although the rating of the laboratory prototype is lower than the practical high-power drive, their key parameters are similar. A dc motor is coupled to the shaft of the induction machine. It is supplied by a dc drive to generate the step load torque.

The same time constant is adopted for the speed controller and the induction motor initially operates at zero speed with no load. The stator current is mainly used to generate the flux and its frequency is almost zero. A 0.5 p.u. step load torque is applied and typical waveforms (dc-link current $i_{\rm dc}$, IM phase current

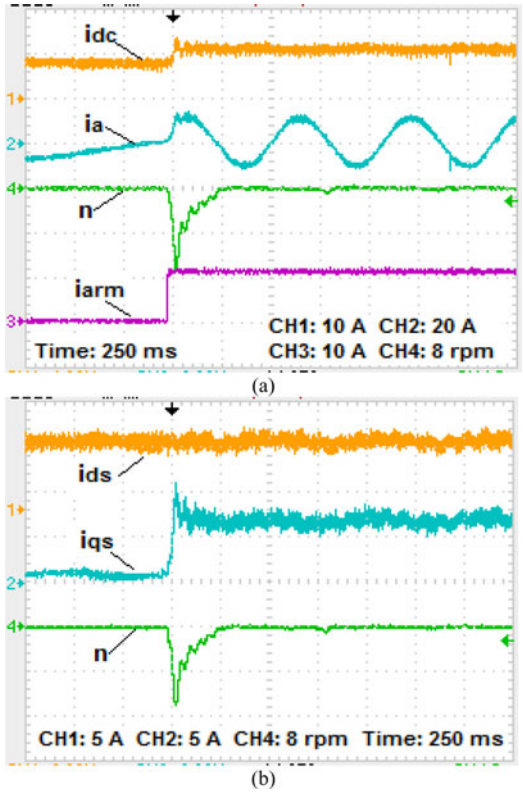

Fig. 12. Experimental waveforms under 0.5 p.u. step torque variation. (a) DC-link current, IM current, dc motor armature current. (b) IM stator d-axis current, q-axis current, and speed.

i_a, dc motor armature current $i_{\rm arm}$, stator d-axis current i_{ds}, stator q-axis current i_{qs}, and speed n) are shown in Fig. 12. The dc motor field flux is constant and the armature current $i_{\rm arm}$ represents the load torque addressed on the induction motor. Once the load torque is addressed, the stator q-axis current increases quickly while d-axis current varies little. The dc-link current, which is controlled for the stator current amplitude regulation in Fig. 2, is increased accompanying one cycle of oscillation. The motor speed decreases to -14.4 r/min and then recovers to zero. At steady state, the stator current frequency is nearly 1.7 Hz, which is half of rated slip frequency.

By employing the load torque feedforward control, the system performance under 0.5 p.u. step load torque is shown in Fig. 13. Due to the faster speed response, the dc-link current and stator q-axis current exhibit more transient resonances, while the motor speed drop is reduced to 8 r/min. The speed recovery overshoot is increased as well, from 0 to 2.5 r/min. In the meantime, the q-axis current exhibits a small amount of LF ripples after the implementation of the feedforward control, which is not presented in the simulation results. This is mainly introduced by the speed derivative, which highly depends on the encoder resolution and measurement noises. A comparatively large time constant τ is adopted for the low-pass filter to suppress such effect, which contributes to larger speed recovery overshoot, as shown in Fig. 13(b).

With 1 p.u. step torque variation, the system performance without and with the load torque observer are show in Figs. 14

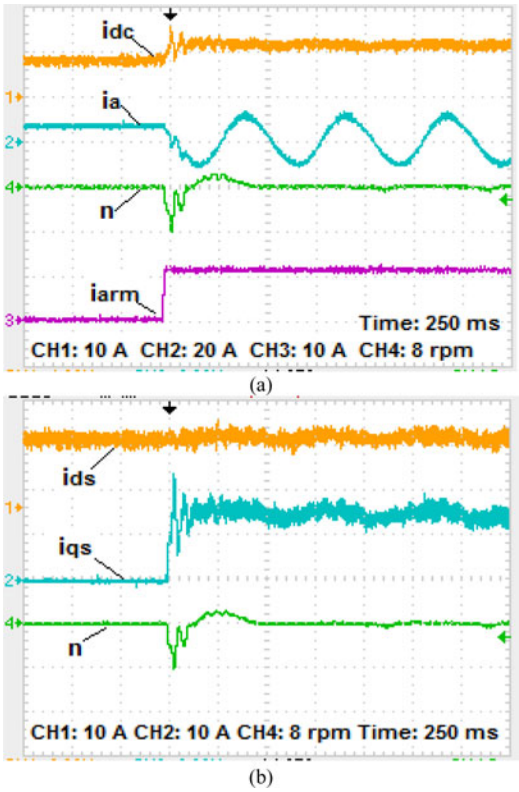

Fig. 13. Experimental waveforms under 0.5 p.u. step torque variation (with load torque feedforward control). (a) DC-link current, IM current, dc motor armature current. (b) IM stator d-axis current, q-axis current, and speed.

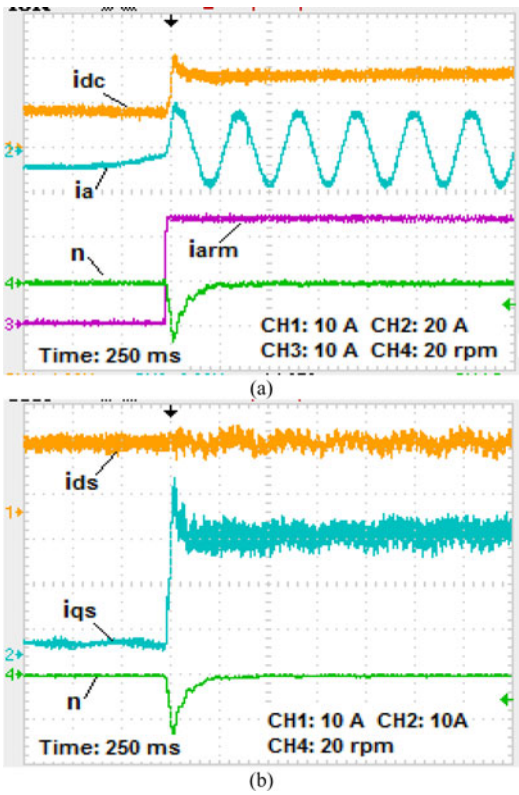

Fig. 14. Experimental waveforms under 1 p.u. step torque variation. (a) DC-link current, IM current, dc motor armature current. (b) IM stator d-axis current, q-axis current, and speed.

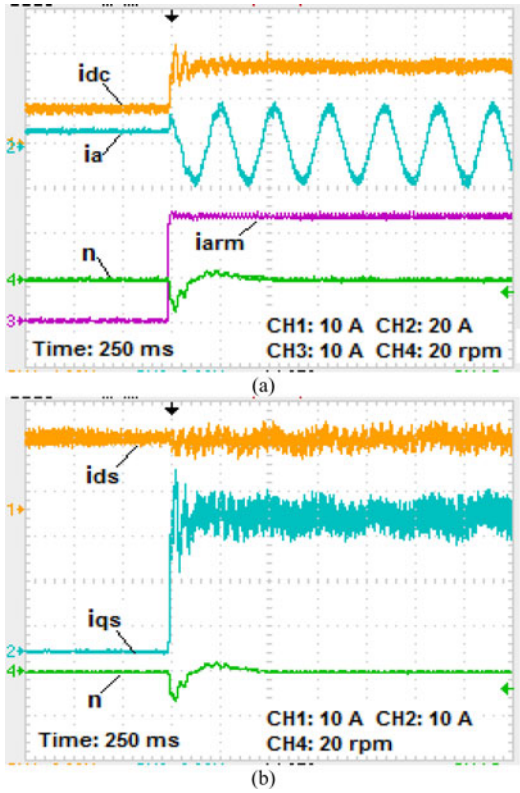

Fig. 15. Experimental waveforms under 1 p.u. step torque variation (with load torque feedforward control). (a) DC-link current, IM current, dc motor armature current. (b) IM stator d-axis current, q-axis current, and speed.

and 15, respectively. Without the load torque observer, the dc-link current and stator d, q-axis currents exhibit almost no transient oscillations due to comparatively slow speed response. The speed drop is up to 28 r/min. With the help of load torque observer, the speed drop is reduced to 14 r/min, while the dc-link current and stator d, q-axis currents suffer about two cycles of transient resonance.

VI. Conclusion

In this paper, the zero-speed operation of PWM CSI-fed IMD with speed senor is investigated. The motor is controlled with rotor flux orientation, where the rotor flux is estimated using stator currents and motor speed. Due to the CSI-side filter capacitors, the stator currents are a portion of the inverter output currents. The influence of these capacitors on the motor control performance is systematically evaluated. A load torque observer with feedforward control is also utilized to improve the speed dynamic response. Simulation and experiments show that the CSI-fed IMD works well at zero speed with promising speed dynamic performance.

References

[1] Y. W. Li, M. Pande, N. R. Zargari, and B. Wu, "Dc-link current minimization for high-power current-source motor drives," *IEEE Trans. Power Electron.*, vol. 24, no. 1, pp. 232–240, Jan. 2009.

[2] A. Weber, P. Kern, and T. Dalibor, "A novel 6.5 kV IGCT for high power current source inverters," in *Proc. Int. Symp. Power Semicond. Devices ICs*, Osaka, Japan, 2001, pp. 215–218.

[3] N. R. Zargari, S. C. Rizzo, Y. Xiao, H. Iwamoto, K. Satoh, and J. F. Donlon, "A new current-source converter using a symmetric gate-commutated thyristor (SGCT)," *IEEE Trans. Ind. Appl.*, vol. 37, no. 3, pp. 896–903, May/Jun. 2001.

[4] Y. W. Li, M. Pande, N. R. Zargari, and B. Wu, "An input power factor control strategy for high-power current-source induction motor drive with active front-end," *IEEE Trans. Power Electron.*, vol. 25, no. 2, pp. 352–359, Feb. 2010.

[5] J. D. Ma, B. Wu, N. R. Zargari, and S. C. Rizzo, "A space vector modulated CSI-based ac drive for multimotor applications," *IEEE Trans. Power Electron.*, vol. 16, no. 4, pp. 535–544, Jul. 2001.

[6] A. Klonne and F. W. Fuchs, "High dynamic performance of a PWM current source converter induction machine drive," in *Proc. 10th Eur. Conf. Power Electron. Appl.*, 2003, pp. 1–10.

[7] V. D. Colli, P. Cancelliere, F. Marignetti, and R. D. Stefano, "Influence of voltage and current source inverters on low-power induction motors," *IEE Proc. Electr. Power Appl.*, vol. 152, no. 5, pp. 1311–1320, Sep. 2005.

[8] M. Salo and H. Tuusa, "A vector-controlled PWM current-source-inverter-fed induction motor drive with a new stator current control method," *IEEE Trans. Ind. Electron.*, vol. 52, no. 2, pp. 523–531, Apr. 2005.

[9] M. H. Bierhoff and F. W. Fuchs, "Active damping for three-phase PWM rectifiers with high-order line-side filters," *IEEE Trans. Ind. Electron.*, vol. 56, no. 2, pp. 371–379, Feb. 2009.

[10] Z. Bai, X. Ruan, and Z. Zhang, "A generic six-step direct PWM (SS-DPWM) scheme for current source converter," *IEEE Trans. Power Electron.*, vol. 25, no. 3, pp. 659–666, Mar. 2010.

[11] Y. W. Li, B. Wu, D. Xu, and N. R. Zargari, "Space vector sequence investigation and synchronization methods for active front-end rectifiers in high-power current-source drives," *IEEE Trans. Ind. Electron.*, vol. 55, no. 3, pp. 1022–1034, Mar. 2008.

[12] L. A. C. Lops and M. F. Naguib, "Space-vector-modulated hybrid bidirectional current source converter," *IEEE Trans. Power Electron.*, vol. 25, no. 4, pp. 1055–1067, Apr. 2010.

[13] R. T. H. Li, H. S. Chung, W. Lau, and B. Zhou, "Use of hybrid PWM and passive resonant snubber for a grid-connected CSI," *IEEE Trans. Power Electron.*, vol. 25, no. 2, pp. 298–309, Feb. 2010.

[14] D. Banerjee and V. T. Ranganathan, "Load-commutated SCR current-source-inverter-fed induction motor drive with sinusoidal motor voltage and current," *IEEE Trans. Power Electron.*, vol. 24, no. 4, pp. 1048–1061, Apr. 2009.

[15] K. Hatua and V. T. Ranganathan, "A novel VSI and CSI fed dual stator induction motor drive topology for medium voltage drive applications," *IEEE Trans. Power Electron.*, vol. 58, no. 8, pp. 3373–3382, Aug. 2011.

[16] P. Tenca, A. A. Rockhill, T. A. Lipo, and P. Tricoli, "Current source topology for wind turbines with decreased mains current harmonics, further reducible via functional minimization," *IEEE Trans. Power Electron.*, vol. 23, no. 3, pp. 1143–1155, May 2008.

[17] A. R. Beig and V. T. Ranganathan, "A novel CSI-fed induction motor drive," *IEEE Trans. Power Electron.*, vol. 21, no. 4, pp. 1073–1072, Jul. 2006.

[18] Y. Suh, J. Steinke, and P. Steimer, "A study on efficiency of voltage source and current source converter systems for large motor drives," in *Proc. 37th IEEE Power Electron. Spec. Conf.*, 2006, pp. 1–7.

[19] E. P. Wiechmann, P. Aquevenque, R. Burgos, and J. Rodriguez, "On the efficiency of voltage source and current source inverters for high-power drives," *IEEE Trans. Ind. Electron.*, vol. 55, no. 4, pp. 1771–1782, Apr. 2008.

[20] B. Wu, *High-Power Converters and AC Drives*. Hoboken, NJ: Wiley, 2006.

[21] D. N. Zmood and D. G. Holmes, "Improved voltage regulation for current-source inverters," *IEEE Trans. Ind. Appl.*, vol. 37, no. 4, pp. 1028–1036, Jul./Aug. 2001.

[22] B. K. Bose, *Modern Power Electronics and AC Drives*. Englewood Cliffs, NJ: Prentice-Hall, 2002.

[23] J. Liao and S. Yeh, "A novel instantaneous power control strategy and analytic model for integrated rectifier/inverter systems," *IEEE Trans. Power Electron.*, vol. 15, no. 6, pp. 996–1006, Nov. 2000.

[24] M. Iwasaki and N. Matsui, "Robust speed control of IM with torque feedforward control," *IEEE Trans. Ind. Electron.*, vol. 40, no. 6, pp. 553–562, Dec. 1993.

Fangrui Liu (M'11) received the B.Eng. degree in electrical engineering from Huazhong University of Science and Technology, Wuhan, China, in 2002, and the Ph.D. degree from Nanyang Technological University, Singapore, in 2006.

Since September 2006, he has been with the College of Electrical and Electronic Engineering, Huazhong University of Science and Technology, where he has been a Lecturer since September 2008. He is currently a Postdoctoral Fellow in the Department of Electrical and Computer Engineering, Ryerson University, Toronto, ON, Canada. His research includes power converters, ac motor drives, and renewable energy resources.

Bin Wu (S'89–M'92–SM'99–F'08) received the M.A.Sc. and Ph.D. degrees in electrical and computer engineering from the University of Toronto, Toronto, ON, Canada, in 1989 and 1993, respectively.

After being with Rockwell Automation Canada as a Senior Engineer, he joined Ryerson University, Toronto, ON, Canada, where he is currently a Professor and the Natural Sciences and Engineering Research Council of Canada (NSERC)/Rockwell Industrial Research Chair in Power Electronics and Electric Drives. He is the author or coauthor of more than 200 technical papers, author/coauthor of two Wiley-IEEE Press books, and holds more than 20 issued/pending patents in the area of power conversion, advanced controls, adjustable speed drives, and renewable energy systems.

Dr. Wu received the Gold Medal of the Governor General of Canada, the Premier's Research Excellence Award, Ryerson Distinguished Scholar Award, Ryerson Research Chair Award, and the NSERC Synergy Award for Innovation. He is a Fellow of the Engineering Institute of Canada and the Canadian Academy of Engineering. He is an Associate Editor of the IEEE TRANSACTIONS ON POWER ELECTRONICS and IEEE Canadian Review.

Manish Pande (S'92–M'93) received the B.Eng. degree from Anna University, Chennai, India, in 1991, the M.A.Sc. degree from Concordia University, Montreal, QC, Canada, in 1994, and the Ph.D. degree from the University of Toronto, Toronto, ON, Canada, in 1998.

Since August 1997, he has been with the Medium Voltage R&D Department, Rockwell Automation, Cambridge, ON, first as a Senior Designer and then as the Team Leader of the hardware and software development team looking after the design and development of modern control systems for various generations of medium-voltage ac drives. His research interests include ac motor drives, high-power converter topologies, and control system design.

Navid Reza Zargari (M'95–SM'03) received the B.Eng. degree from Tehran University, Tehran, Iran, in 1987, and the M.A.Sc. and Ph.D. degrees from Concordia University, Montreal, QC, Canada, in 1991 and 1995, respectively.

Since November 1994, he has been with the Medium Voltage R&D Department, Rockwell Automation, Cambridge, ON, Canada, first as a Senior Designer and currently as the Manager of the same department. Since 15 years, he has been involved in research on simulation, analysis, and design of power converters for medium-voltage ac drives. He is the coauthor of more than 50 research papers and holds 8 US patents. His research interests include power converter topologies and their control aspects, high-power-factor three-phase rectifiers, var compensators, power semiconductors, and renewable energy sources.

Dr. Zargari is registered as a Professional Engineer in the Province of Ontario.